LANGMUIR

Article

pubs.acs.org/Langmuir

Nanoparticle-Induced Ellipse-to-Vesicle Morphology Transition of Rod−Coil−Rod Triblock Copolymer Aggregates

Chaoying Yang, Qing Li, Chunhua Cai,* and Jiaping Lin*

Shanghai Key Laboratory of Advanced Polymeric Materials, State Key Laboratory of Bioreactor Engineering, Key Laboratory for Ultrafine Materials of Ministry of Education, School of Materials Science and Engineering, East China University of Science and Technology, Shanghai 200237, China

Supporting Information

ABSTRACT: Cooperative self-assembly behavior of rod−coil−rod poly(γ-benzyl-L-glutamate)-*block*-poly(ethylene glycol)-*block*-poly(γ-benzyl-L-glutamate) (PBLG-*b*-PEG-*b*-PBLG) amphiphilic triblock copolymers and hydrophobic gold nanoparticles (AuNPs) was investigated by both experiments and dissipative particle dynamics (DPD) simulations. It was discovered that pure PBLG-*b*-PEG-*b*-PBLG copolymers self-assemble into ellipse-like aggregates, and the morphology transforms into vesicles as AuNPs are introduced. When the hydrophobicity of AuNPs is close to that of the copolymers, AuNPs are homogeneously distributed in the vesicle wall. While for the AuNPs with higher hydrophobicity, they are embedded in the vesicle wall as clusters. In addition to the experimental observations, DPD simulations were performed on the self-assembly behavior of triblock copolymer/nanoparticle mixtures. Simulations well reproduced the morphology transition observed in the experiments and provided additional information such as chain packing mode in aggregates. It is deduced that the main reason for the ellipse-to-vesicle transition of the aggregates is attributed to the breakage of ordered and dense packing of PBLG rods in the aggregate core by encapsulating AuNPs. This study deepens our understanding of the self-assembly behavior of rod−coil copolymer/nanoparticle mixtures and provides strategy for designing hybrid polypeptide nanostructures.

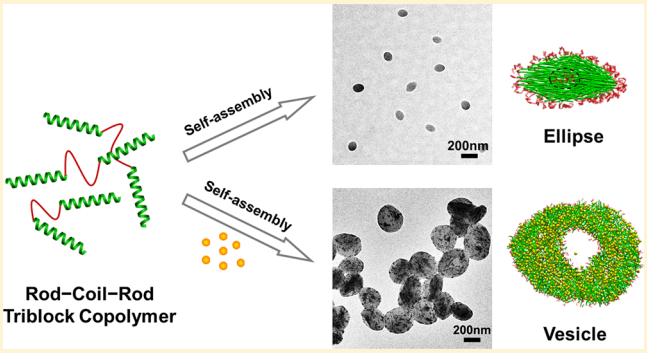

INTRODUCTION

Amphiphilic block copolymers (BCPs) are able to self-assemble into various supramolecular aggregates in selective solvents, such as spheres, rods, vesicles, toroids, and other complex structures.[1−4] These structures have attracted widespread interests for their potential usages as drug delivery system, nanoreactor, additive for mineralization of inorganics, and so on.[5−8] Introduction of nanoparticles (NPs) can regulate the self-assembly structure and endow the self-assembled aggregates with novel functions including optical, electrical, magnetic, biological, and mechanical properties.[9−11] Research on cooperative self-assembly of BCPs and NPs not only enriches our knowledge in the supramolecular science but also benefits for designing and constructing functional materials.

Generally, the role of NPs in copolymer/NPs cooperative self-assembly systems can be classified into two types. One is that the NPs act as surface template to guide the assembly of BCPs.[12] In another type, the NPs act as modifier to regulate the structure of assemblies.[13−17] For example, Park et al. found that incorporation of iron oxide NPs can induce a vesicle-to-micelle or micelle-to-vesicle morphology transition of polystyrene-*block*-poly(acrylic acid) (PS-*b*-PAA) BCP assemblies.[13] Moreover, they demonstrated that one can control the location of NPs in copolymer assemblies by property of surface ligands of NPs.[14] Apart from experimental investigations, theory simulations have emerged as powerful tools to study the self-assembly behaviors of block copolymer/nanoparticle mixtures.[18−21] For example, Zhang et al. used self-consistent field theory (SCFT) to investigate the self-assembly of BCP/NPs.[18] It was found that the volume fraction of NPs, the ratio of NP radius to BCP chain gyration radius, and the surface selectivity of NPs to blocks play important roles in the self-assembly behaviors. Their simulation results are well confirmed by experimental findings.[16,18,19]

However, so far most studies are focused on coil−coil type BCPs; rod−coil type BCPs are rarely referred in the cooperative self-assembly of BCPs with NPs. As compared to coil−coil BCPs, the rod−coil BCPs exhibit distinct self-assembly behaviors because the rod blocks prefer to take ordered packing mode in the aggregates.[22−32] For instance, Wan et al. investigated the self-assembly behavior of rod−coil diblock copolymers based on poly(ethylene oxide) (PEO) and poly{(+)-2,5-bis[4′-((*S*)-2-methylbutoxy)phenyl]styrene} (PMBPS), PEO_{104}-*b*-$PMBPS_{53}$ in THF/water and dioxane/

Received: April 18, 2016
Revised: May 30, 2016
Published: June 17, 2016

DOI: 10.1021/acs.langmuir.6b01484
Langmuir 2016, 32, 6917−6927

water, respectively.[27] The orientational order of the rigid PMBPS blocks leads to the anisotropic disclike aggregates in THF/water. Liu et al. reported the self-assembly behavior of a triblock terpolymer containing a rigid liquid crystalline block.[28] It was found that polygonal cylindrical micelles bearing sharp bends can be formed. This type of morphology is ascribed to the ordered packing of rigid liquid crystalline blocks in the core of the cylinder. These examples demonstrated that ordering of rigid blocks is a critical factor influencing the self-assembly behaviors of rod−coil block copolymers. Therefore, it is expected that the change of the ordered packing of rigid blocks should greatly affect the self-assembly behaviors of rod−coil copolymers.[33] As a matter of fact, for example, as observed in the homopolymer liquid crystal systems, the ordered packing of rigid polymer chains can be destroyed by introducing a small portion of NPs.[34] So far, limited attention has been devoted to the effect of NPs on the self-assembly behavior of rod−coil block copolymers in solution.

On the other hand, recently increasing attention has been paid to the self-assembly behaviors of polypeptide-based block and graft copolymers.[35−41] Understanding their supramolecular assembly behaviors could be helpful for knowing the complex aggregation behaviors of polypeptides in organisms due to their analogous component with natural proteins. In addition, polypeptides can adopt a rigid α-helix conformation and are usually used as a model of rigid polymer segments.[38] Researches on the self-assembly behaviors of mixture systems comprising polypeptide-based rod−coil block copolymers and NPs can not only deepen the understanding of the self-assembly behavior of rod−coil copolymers but also help the investigation of complex protein systems.

In the present work, we investigated cooperative self-assembly behavior of amphiphilic poly(γ-benzyl-L-glutamate)-*block*-poly(ethylene glycol)-*block*-poly(γ-benzyl-L-glutamate) (PBLG-*b*-PEG-*b*-PBLG) rod−coil−rod triblock copolymers with hydrophobic gold nanoparticles (AuNPs) in aqueous solution. Pure triblock copolymers with relatively longer PBLG rods self-assemble into ellipse-like aggregates. When AuNPs were introduced, vesicles were formed. The AuNPs were found to be distributed in the vesicle wall. The effects of size and hydrophobicity of the AuNPs were studied. In addition to experimental studies, dissipative particle dynamics (DPD) simulations on the cooperative self-assembly of model rod−coil−rod triblock copolymer and NPs were performed to examine the morphology transition. On the basis of the experimental findings and DPD simulation results, the mechanism of morphology transition of rod−coil−rod triblock copolymers induced by AuNPs is suggested.

EXPERIMENTAL SECTION

Materials. *O*,*O*′-Bis(2-aminoethyl)poly(ethylene glycol) (H_2N-PEG-NH_2, M_n = 6000), gold(III) chloride trihydrate ($HAuCl_4 \cdot 3H_2O$, >99.9%), and sodium borohydride ($NaBH_4$, ≥98.0%) were purchased from Sigma-Aldrich. Oleylamine (OAm, C18 content: 80%−90%) was purchased from Acros Organics. γ-Benzyl-L-glutamate-*N*-carboxyanhydride (BLG-NCA) was synthesized according to the literature.[42] Analytical grade of 1,4-dioxane was refluxed with sodium and distilled immediately before use. All the other reagents are of analytical grade and used as received. Dialysis bag (Membracel, 3500 molecular weight cutoff) was provided by Serva Electrophoresis GmbH.

Synthesis of PBLG-*b*-PEG-*b*-PBLG Triblock Copolymers and Gold Nanoparticles. PBLG-*b*-PEG-*b*-PBLG (abbreviated as BEB) triblock copolymers were synthesized in anhydrous 1,4-dioxane solution using ring-opening polymerization of BLG-NCA initiated by the terminal amino groups of H_2N-PEG-NH_2.[29,42] Three types of gold nanoparticle (AuNPs) were synthesized according to the literature,[43−45] i.e., oleylamine-stabilized small AuNPs (AuOAm1), oleylamine-stabilized large AuNPs (AuOAm2), and 1-dodecanethiol-stabilized small AuNPs (AuDT). The details for the synthesis of BEB and AuNPs are provided in section 1 of the Supporting Information.

Preparation of Aggregates from BEB Triblock Copolymers and AuNPs Mixtures. The polymeric aggregates were prepared using a dialysis method.[24,37] BEB and AuNPs were first dissolved/dispersed in THF separately with initial concentration of 1.0 g/L. In a following step, 1.2 mL of polymer solution and various volumes (0.1−2.0 mL) of AuNPs solutions were mixed together to obtain stock solutions. The stock solutions were then diluted with THF to 4.0 mL; thus, the polymer concentration was 0.3 g/L, and the AuNPs concentration was 0.025−0.5 g/L. To prepare aggregate solutions, 2.0 mL of water, a selective solvent for PEG, was added at a rate of ca. 0.5 mL/min with vigorous stirring. After further stirring for 2 h, 15.0 mL of deionized water was injected to the solution. Finally, the solution was dialyzed against deionized water for 3 days to remove the organic solvents. All the assembling and dialysis processes were conducted at room temperature. Before analysis, the micelle solutions were stabilized for at least 5 days.

Turbidity Measurements (OD). Turbidity measurements were performed to determine the critical water content for the aggregation of polymers or AuNPs.[29,31] The polymers or AuNPs solution/dispersion in THF was charged into a quartz cell (path length: 1 cm). Deionized water was then added drop by drop (0.02 mL per drop to 2.0 mL of solution) with stirring. After the deionized water was added, the solution was stirred for 1 min and left to equilibrate for 2 min or more until the recorded optical density was stable. The optical density (turbidity) was measured at a wavelength of 700 nm (which was far from the absorption of the benzene chromophore) with a UV−vis spectrophotometer (UV−vis UV-2550, Shimadzu).

Transmission Electron Microscopy (TEM). The morphologies of the AuNPs and self-assembled aggregates were examined by TEM (JEM-2100F, JEOL) operated at an accelerating voltage of 200 kV. Drops of solution were placed on a copper grid coated with carbon film and then were dried at room temperature.

Scanning Electron Microscopy (SEM). The morphologies of the aggregates were also observed by SEM (S4800, Hitachi) operated at an accelerating voltage of 15 kV. The samples were prepared by placing drops of solution on a copper grid coated with carbon film and then were dried at room temperature. Before the observations, the samples were sputtered by Aurum.

Atom Force Microscopy (AFM). AFM measurements were performed with XE-100 (Park Systems) by using the noncontact mode at room temperature in air. The samples were prepared by placing drops of solution on a silicon wafer surface and allowed to dry in air.

Laser Light Scattering Measurements (LLS). The structure of the aggregates was characterized by combining dynamic (DLS) and static light scattering (SLS) measurements, which were performed on a commercial LLS spectrometer (ALV/CGS-5022) equipped with an ALV-High QE APD detector and an ALV-5000 digital correlator using a He−Ne laser (the wavelength λ = 632.8 nm) as light source. All the measurements were carried out at room temperature, and the samples were diluted before measurement. From DLS testing, hydrodynamic radius ($\langle R_h \rangle$) can be obtained, which indicates the radius of a hard sphere with the same translational diffusion coefficient and the same condition. While the SLS measurements gives the radius of gyration ($\langle R_g \rangle$), which reflects the density distribution of the aggregates in real physical space.

Dissipative Particle Dynamics (DPD) Simulations. The DPD simulations were conducted to illuminate the structures of ellipse-like aggregates and vesicles. Details of DPD and the choice of simulation parameters can be found in our previous works.[4,29,33] A DPD model of symmetric rod−coil−rod triblock copolymer was constructed to simulate the $PBLG_{283}$-*b*-PEG_{136}-*b*-$PBLG_{283}$ copolymers synthesized in the experiments (Figure S7). The triblock copolymer model consists of ten **R** beads on each rod block and three **C** beads on each coil block

DOI: 10.1021/acs.langmuir.6b01484
Langmuir 2016, 32, 6917−6927

(denoted by $\mathbf{R}_{10}\mathbf{C}_3\mathbf{R}_{10}$).[29] The DPD beads in each rod block were linearly arranged and restricted to move as a rigid body. The distance between neighbor **R** beads was set as 0.86 r_c. The coil block was modeled as a flexible polymeric chain. The current choice of block lengths corresponds to the experiments, where the length of PBLG is longer than that of PEG. More detailed information regarding the setting of model parameters is given in section 6.1 of the Supporting Information. The solvent bead was modeled as a single bead and denoted by **S** (not shown). The smaller (~4.5 nm) and larger (~18.9 nm) AuNPs were modeled as a single DPD bead and a rigid icosahedron (radius equal to 1.0 r_c), respectively. Nanoparticles were denoted by **N**. The units of length, time, mass, and energy in our simulations were defined by r_c, τ, m, and k_BT, respectively. The time unit τ was obtained by $\tau = (mr_c^2/k_BT)^{1/2}$, and its real value can be evaluated via matching the simulated lateral diffusion coefficient with the value measured in experiments. All simulations in the present work were carried out in 40 × 40 × 40 r_c^3 cubic boxes with periodic boundary conditions. The NVT ensemble was adopted. The interaction parameter a_{ij} between DPD beads is given in Table 1 (the detailed information on the choice of a_{ij} is given in section 6.2 of the Supporting Information). The time integration of motion equations was done by a modified velocity-Verlet algorithm, with the time step $\Delta t = 0.04\tau$. Six ×10^5 DPD steps were carried out in our simulations to ensure the simulation time long enough for the systems to achieve equilibrium states.

Table 1. Interaction Parameter a_{ij} Used in the DPD Simulation

a_{ij}	R	C	P	S
R	25	30−75	25−75	30−75
C		25	30−200	25
P			25	30−200
S				25

The ordered packing of rod blocks inside an ellipse can be characterized by the angles between the rod blocks and the long axis of the ellipse (see the insets of Figure 2g). The angle θ_i corresponding to the ith rod block is defined by

$$\theta_i = \cos^{-1}|\mathbf{u}_i \cdot \mathbf{u}_d| \quad (1)$$

where $\mathbf{u}_i$ is the normalized vector of the ith rod and $\mathbf{u}_d$ is the normalized vector of the long axis of the ellipse. The average θ for an arbitrary point inside a simulated ellipse was computed as follows. First, we computed the value of θ for every rod block inside the ellipse core. Then, for an arbitrary point **r**, we figured out those rod blocks whose distance from **r** is within a critical value d_c. (Herein we choose $d_c = r_c$.) Finally, the values of θ corresponding to these rod blocks were averaged to get the average θ for point **r**.

In addition, the degree of nematic ordering in aggregates was characterized by the order parameter S.[46] The order parameter S_i for the ith rod is given by

$$S_i = \frac{3(\mathbf{u}_i \cdot \mathbf{u}_d)^2 - 1}{2} \quad (2)$$

where $\mathbf{u}_i$ is the normalized vector of the ith rod (from the first bead to the last bead) and $\mathbf{u}_d$ is the normalized vector of orientation direction, which is determined by iteration to find the largest value of S. The

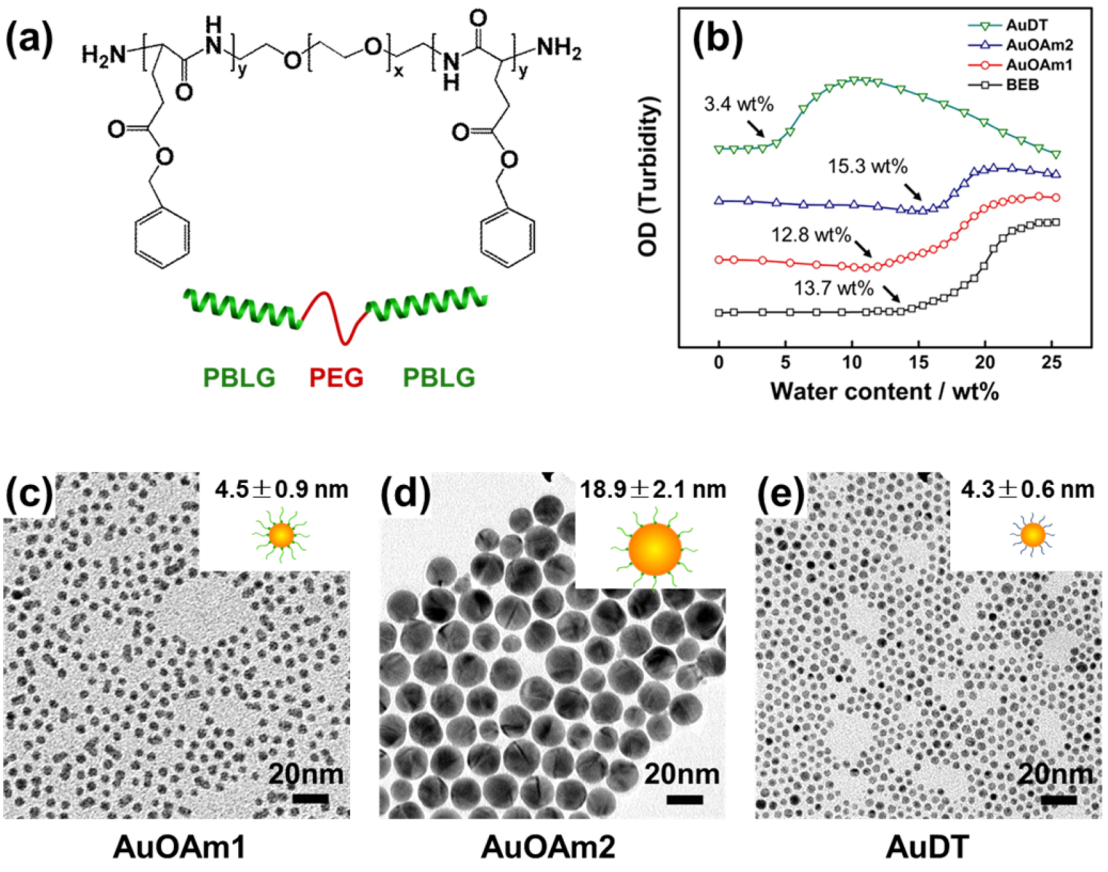

Figure 1. (a) Molecular structure and schematic model of PBLG-*b*-PEG-*b*-PBLG (BEB) triblock copolymer. (b) Turbidity curves of BEB triblock copolymer and three types of AuNPs in THF as a function of the amount of water added to the solution. The arrows indicate the CWC points of the corresponding BEB and AuNPs solutions. (c−e) TEM images of AuNPs with different diameters and ligands. (c, d) AuNPs coated with oleylamine (AuOAm1 and AuOAm2); the diameters are 4.5 ± 0.9 and 18.9 ± 2.1 nm, respectively. (e) AuNPs coated with 1-dodecanethiol (AuDT); the diameter is 4.3 ± 0.6 nm. Insets in TEM images show the cartoon pictures of the AuNPs.

DOI: 10.1021/acs.langmuir.6b01484
Langmuir 2016, 32, 6917−6927

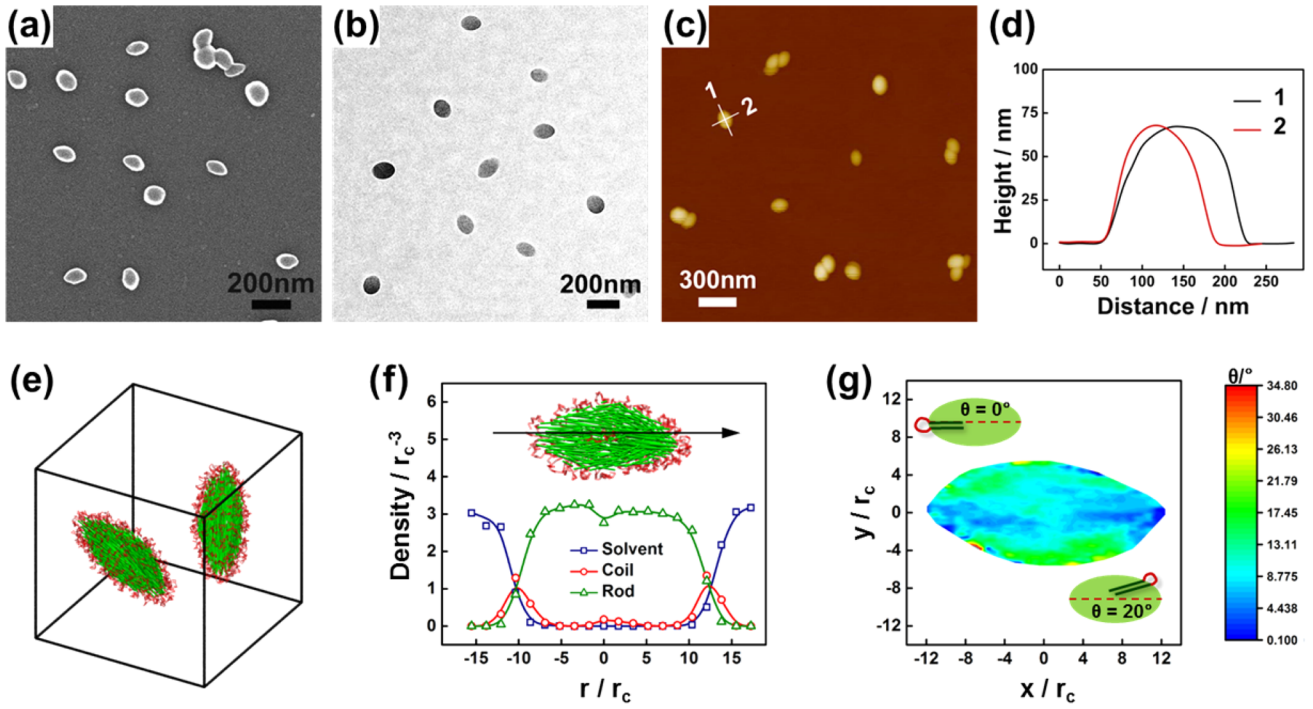

Figure 2. (a) SEM, (b) TEM, and (c) AFM images of the ellipse-like aggregates self-assembled from BEB triblock copolymers. (d) Height profiles along the white line 1 and line 2 in (c). (e) Equilibrium morphology of ellipse-like aggregates obtained by a DPD simulation. The rod blocks and coil blocks are colored by green and red, respectively. (f) Density profiles of rod blocks, coil blocks, and solvents along the long axis (denoted by the black arrow) of a typical simulated ellipse. (g) Distribution of average angles θ between normalized vectors of rod blocks and long axis of ellipse-like aggregates. x and y correspond to the positions along the long axis and short axis of the aggregates, respectively. Insets at the upper left corner and lower right corner show two typical copolymers with their rod blocks parallel to the long axis (θ = 0°) and inclined to the long axis (θ = 20°), respectively. Color bar at the right side shows the scale of θ.

order parameter S of rod blocks within the aggregate is the average value of S_i.

RESULTS AND DISCUSSION

Characterization of PBLG-*b*-PEG-*b*-PBLG Triblock Copolymers and Gold Nanoparticles. Figure 1a shows the molecular structure of BEB triblock copolymer. Since PBLG blocks take rigid α-helix conformation (Figure S1), the BEB triblock copolymer can be modeled as rod−coil−rod polymeric system. The degree of polymerization (DP) of PEG block is known to be 136, and the DP of each PBLG block is 283 according to NMR analysis. GPC analysis in DMF reveals a monomodal symmetric distribution with a relatively narrow PDI value of 1.25 (Figure S2), which indicates a well-controlled polymerization process. In addition, PBLG-*b*-PEG-*b*-PBLG triblock copolymers with the same PEG block length but various PBLG block lengths were synthesized, for example, $PBLG_{103}$-*b*-PEG_{136}-*b*-$PBLG_{103}$, $PBLG_{170}$-*b*-PEG_{136}-*b*-$PBLG_{170}$, and $PBLG_{434}$-*b*-PEG_{136}-*b*-$PBLG_{434}$. The subscripts denote the DP for each block. The detailed characterizations for these triblock copolymers were presented in Supporting Information (Section 2, Table S1).

Figures 1c−e show the TEM images of the AuNPs. Spherical morphology was observed for these AuNPs, and the average diameters are 4.5 ± 0.9 nm for AuOAm1, 18.9 ± 2.1 nm for AuOAm2, and 4.3 ± 0.6 nm for AuDT (Figure S3). The insets in each image are the cartoons of the AuNPs. The different ligand molecules induce different hydrophobicity (or surface properties) of AuNPs, which may lead to distinct cooperative self-assembly behaviors as well as the distributions of NPs in hydrophobic domains of the aggregates.[14,47]

The triblock copolymers and AuNPs are soluble/dispersible in THF, and adding water can induce the aggregation of copolymers or AuNPs. The aggregation process can be monitored by turbidity testing.[29,31] From the turbidity curves shown in Figure 1b, one can see that the onset of the aggregation for BEB occurs at water content (critical water content, CWC) of 13.7 wt %. And for AuNPs, the CWCs are 12.8 wt % for AuOAm1, 15.3 wt % for AuOAm2, and 3.4 wt % for AuDT. The CWC value reflects the hydrophobicity of copolymers and AuNPs. The results suggest that both AuOAm1 and AuOAm2 possess the hydrophobicity close to that of BEB triblock copolymers, while AuDT is much more hydrophobic.

Self-Assembly Behavior of BEB Triblock Copolymers. Pure BEB triblock copolymers self-assembled into ellipse-like aggregates, as observed by SEM, TEM, and AFM (Figure 2). SEM (Figure 2a) and TEM (Figure 2b) images reveal that these ellipse-like aggregates have solid internal structures. The size of the ellipses is not highly uniform, which could be a result of the polydispersity index of BEB.[48] AFM image shows that the length, width, and height of the ellipse are about 160, 127, and 68 nm, respectively (Figure 2c,d). The ellipse is not a common morphology of copolymer assemblies.[49] The ordered packing of PBLG chains in aggregate core should take responsibility for the formation of such morphology. The structure of ellipse-like aggregates was further revealed by DPD simulations on rod−coil−rod model copolymers. As shown in Figure 2e, the ellipse-like aggregates are formed by rod−coil−rod triblock copolymers with their rod blocks constructing the aggregate cores wrapped by coil blocks. To gain insight into the distributions and orientations of the rod blocks, the density

DOI: 10.1021/acs.langmuir.6b01484
Langmuir 2016, 32, 6917−6927

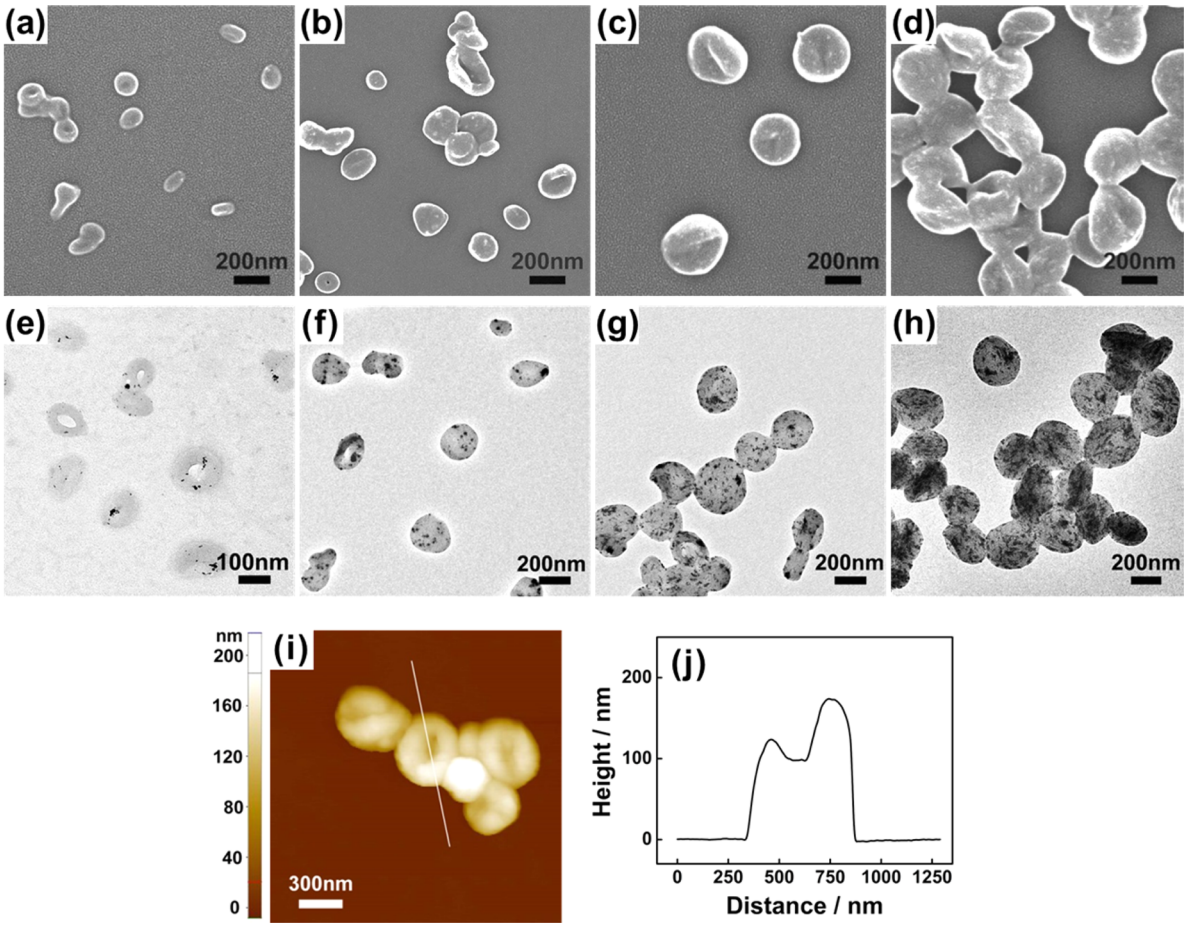

Figure 3. (a–d) SEM and (e–h) TEM images of morphologies of BEB/AuOAm1 mixtures with various nanoparticle weight fractions (f_{OAm1}): (a, e) 0.08, (b, f) 0.14, (c, g) 0.20, (d, h) 0.29. (i) Typical AFM image of vesicles formed by BEB/AuOAm1 mixtures at f_{OAm1} = 0.29. (j) Height profile along the white line in (i).

profiles of respective components and the angle distribution of rod blocks were plotted. As shown in Figure 2f, there are one small peak for the coil blocks and one valley for the rod blocks in the center, indicating that a small amount of coil blocks occupy the aggregate center. However, it is noted that there are no solvents in the aggregate center, which is structurally different from vesicles. The orientation of rod blocks depends on their positions in the aggregates. We measured the orientation of rod blocks by the angle θ between the normalized vectors of rod blocks and the long axis of aggregates (see eq 1). Figure 2g shows the cross section of a typical simulated ellipse-like aggregate with its width and height equal to 24 r_c and 10 r_c, respectively. The color of each point within the ellipse profile represents the average value of θ for this point: a smaller value (blue) indicates that the rod blocks near this point are parallel to the ellipse long axis, whereas a larger value (red) represents that the rod blocks are inclined. Insets of Figure 2g illustrate the relationship between the value of θ and the orientation of a rod block. The result reveals that the rod blocks near the long axis are almost parallel to the long axis of the ellipse, while the rod blocks away from the long axis become tilted. Furthermore, we calculated the order parameter S for the rod blocks within the ellipses (see eq 2). The high value of S (= 0.85) indicates that the rod blocks are oriented and packed regularly within the aggregates.

The effect of PBLG block length on the self-assembly is also examined. It was found that the triblock copolymers with relatively longer PBLG block length, such as $PBLG_{283}$-*b*-PEG_{136}-*b*-$PBLG_{283}$ and $PBLG_{434}$-*b*-PEG_{136}-*b*-$PBLG_{434}$, self-assemble into ellipse-like aggregates. While for the copolymers with shorter PBLG block length ($PBLG_{103}$-*b*-PEG_{136}-*b*-$PBLG_{103}$), vesicles are formed. Such an ellipse-to-vesicle morphology transition is attributed to the fact that the orientation order is reduced as rod blocks become shorter.[29] The details can be found in the Supporting Information (section 4, Figure S4).

Nanoparticle-Induced Ellipse-to-Vesicle Morphology Transitions of Triblock Copolymer Aggregates. To examine the effect of nanoparticle content, cooperative self-assembly behavior of BEB triblock copolymers and AuOAm1 mixtures with various weight fractions of AuOAm1 (f_{OAm1}) was investigated (Figure 3). f_{OAm1} is defined as the ratio of the weight of AuOAm1 to the total weight of triblock copolymer and AuOAm1. As shown in Figure 3a, SEM image reveals that when a little amount of AuOAm1 (f_{OAm1} = 0.08) was introduced, a mixture of ellipse-like aggregates and vesicles was formed. The ellipse-like aggregates are same in the size and shape with those formed by pure BEB triblock copolymers. For the vesicles, TEM image gives a ringlike morphology, which is a typical feature of hard vesicles. Because the wall of vesicle is mainly formed by rigid PBLG blocks, the vesicles may not collapse completely under high vacuum in TEM observations; therefore, a ringlike image was observed.[50,51] As f_{OAm1} increases to 0.14, pure vesicles were formed (Figure 3b). The size of the

DOI: 10.1021/acs.langmuir.6b01484
Langmuir 2016, 32, 6917–6927

vesicle increases with f_{OAm1}. Figures 3c and 3d show SEM images of the vesicles formed at f_{OAm1} = 0.20 and f_{OAm1} = 0.29, respectively. In addition, the vesicles become more uniform in size as f_{OAm1} is increased. From TEM images shown in Figures 3e–h, we can see that the AuNPs disperse homogeneously in the vesicle wall, and the density of the AuNPs increases progressively with f_{OAm1}. AFM testing was applied to further characterize the morphology of the aggregates. Figure 3i shows the typical AFM image of vesicles formed at f_{OAm1} = 0.29. The AFM image displays a higher periphery and lower center of the aggregates, which is a typical image for vesicles.[37,52] As shown in Figure 3j, the height of the lower center (ca. 100 nm) is far smaller than the width of the aggregates (ca. 530 nm), which consists with the feature of collapsed vesicular structure.[52] Note that when the AuOAm1 content is higher than 0.29 (for example, f_{OAm1} = 0.38), uniform vesicles can still be obtained. However, some precipitates were observed in solution. This phenomenon can be attributed to the fact that the higher nanoparticle content increases the volume fraction of hydrophobic part (i.e., PBLG segment *plus* AuOAm1), and the lower volume fraction of hydrophilic PEG segment cannot well support the vesicle.

The "real" aggregate structure in solution was studied by DLS and SLS testing (Figure 4 and Table 2). As shown in

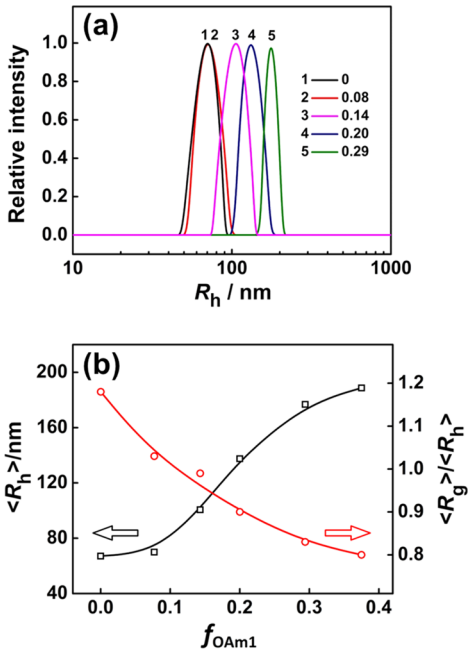

Figure 4. (a) Typical R_h distribution of aggregates formed by BEB/AuOAm1 mixtures with various f_{OAm1} ("1, 2, 3, 4, and 5" denote the corresponding f_{OAm1} of 0, 0.08, 0.14, 0.20, and 0.29, respectively) at the scattering angle of 90°. (b) Plots of $\langle R_h \rangle$ and $\langle R_g \rangle / \langle R_h \rangle$ versus f_{OAm1} for the aggregates formed by BEB/AuOAm1 mixtures.

Figure 4, the average hydrodynamic radius ($\langle R_h \rangle$) of the aggregates was found to increase progressively from 67.1 nm (f_{OAm1} = 0) to 176.8 nm (f_{OAm1} = 0.29). The aggregate structure change can be viewed in terms of the ratio of average radius of gyration $\langle R_g \rangle$ to $\langle R_h \rangle$, which is sensitive to the particle shape.[53,54] Generally, the $\langle R_g \rangle / \langle R_h \rangle$ values for ellipse-like structures, vesicles with a thin layer, vesicles with a wall thickness about 1/3 the radius of the vesicle, and solid spheres are >1.0, 1.0, 0.86, and 0.77, respectively.[54] As can be seen from

Table 2. Typical DLS and SLS Results of Assemblies Formed by BEB/AuOAm1 Mixtures with Various f_{OAm1}

sample	f_{OAm1}	$\langle R_h \rangle$ (nm)	$\langle R_g \rangle$ (nm)	$\langle R_g \rangle / \langle R_h \rangle$	R_h distribution (90°)
BEB/ AuOAm1	0	67.1	79.3	1.18	0.14
	0.08	70.0	72.2	1.03	0.14
	0.14	100.6	99.6	0.99	0.17
	0.20	137.5	124.0	0.90	0.10
	0.29	176.8	146.5	0.83	0.07

Table 2, the $\langle R_g \rangle / \langle R_h \rangle$ value for the ellipse-like aggregates formed by pure BEB copolymers is 1.18. When f_{OAm1} increases to 0.08 and 0.14, the $\langle R_g \rangle / \langle R_h \rangle$ value gradually decreases to about 1.0, which indicates the formation of vesicle. Further increasing AuOAm1 decreases the $\langle R_g \rangle / \langle R_h \rangle$ value, which should be a consequence of increased thickness of the vesicle wall by encapsulating AuOAm1. In addition, all the aggregates possess a narrow size distribution (detected by DLS at the scattering angle of 90°). The LLS results are in good agreement with the morphology observations.

To achieve deep understanding of the cooperative self-assembly behavior of the BEB/AuOAm1 mixtures, we examined the dynamic process of the vesicle formation of the mixtures (f_{OAm1} = 0.29) by monitoring both the turbidity and morphology of the system in the self-assembly. In the experiments, the water was gradually added into initial copolymer/NPs mixture solution, and the obtained results are given in Figure 5. As revealed by turbidity curve, the aggregation occurs at water content around 12.6 wt %. The turbidity increases with the water content and reaches a maximum value at water content about 24.7 wt %. Further increasing water content leads to a slight decrease of the turbidity, which could be a result of the increased volume of the solution. The aggregate morphology at various water contents was observed by SEM. Samples were prepared by transferring a drop of the solution on silicon wafer, frozen by liquid nitrogen, and dried under vacuum. As shown in Figure 5, rodlike aggregates were formed at a low water content of 14.5 wt % (inset a). Increasing water content to 17.7 wt %, vesicles were clearly observed, accompanied by irregular aggregates (inset b). At water content of 22.0 wt %, pure vesicles with diameter about 450 nm were obtained. When water content increases to 28.3 wt %, a decrease in size of the vesicle was observed (about 350 nm, inset d). With further increasing water content, the vesicles become stable and the size does not change obviously. These results indicate that when the added water content reaches CWC value, the mixtures first self-assemble into rodlike primary aggregate with smaller size, analogous to the nucleation process.[55,56] With increasing water content, to lower the interfacial energy, these rod-like primary aggregates evolve to vesicles.

The dynamic process of the vesicle formation was also simulated by DPD. Figure 5e–h shows the equilibrium structures obtained at various solvent conditions. In the simulations, we varied the solvent selectivity parameter from a_{RS} = 30 to a_{RS} = 75 in a step-by-step manner. This process corresponds to adding various amounts of water in the experiments. As can be seen from Figure 5e, the copolymers nucleate and form small spherical micelles when the solvent selectivity is weak. With increasing the solvent selectivity, the small micelles fuse into large micelles and then turn into small vesicles and large vesicles (Figure 5f–h). Therefore, the

DOI: 10.1021/acs.langmuir.6b01484
Langmuir 2016, 32, 6917–6927

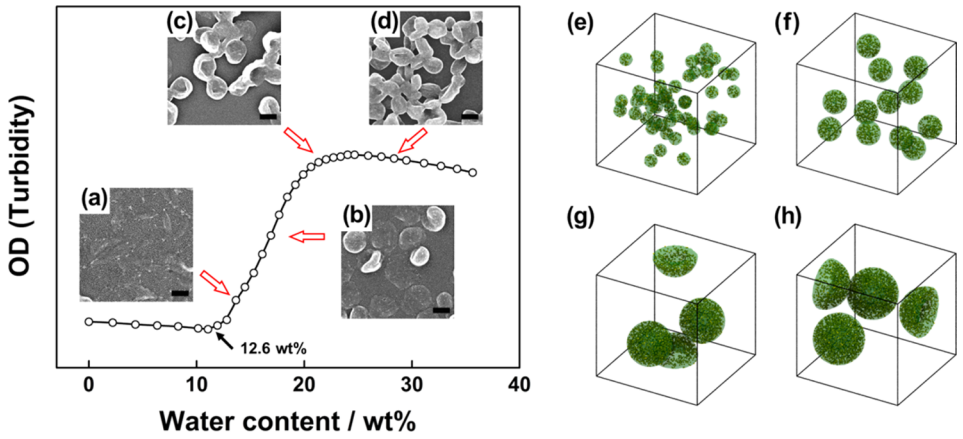

Figure 5. Turbidity curve of BEB/AuOAm1 mixture (f_{OAm1} = 0.29) as a function of the amount of water added to the solution. The insets show the corresponding SEM images of the assemblies formed at various water contents: (a) 14.5 wt %, (b) 17.7 wt %, (c) 22.0 wt %, and (d) 28.3 wt %. No dialysis was performed before SEM observation. Scale bar is 300 nm. (e–h) Equilibrium aggregates obtained from DPD simulations at various solvent conditions (as manifested by variation of a_{RS}): (e) smaller spheres (a_{RS} = 30), (f) larger spheres (a_{RS} = 40), (g) vesicles with moderate size (a_{RS} = 50), and (h) large vesicles (a_{RS} = 75). The weight fraction of NPs in block copolymer/nanoparticle mixtures was set as 0.2. The selectivity of solvent increases gradually from (e) to (h). Only aggregate cores (green) and nanoparticles (yellow) are shown.

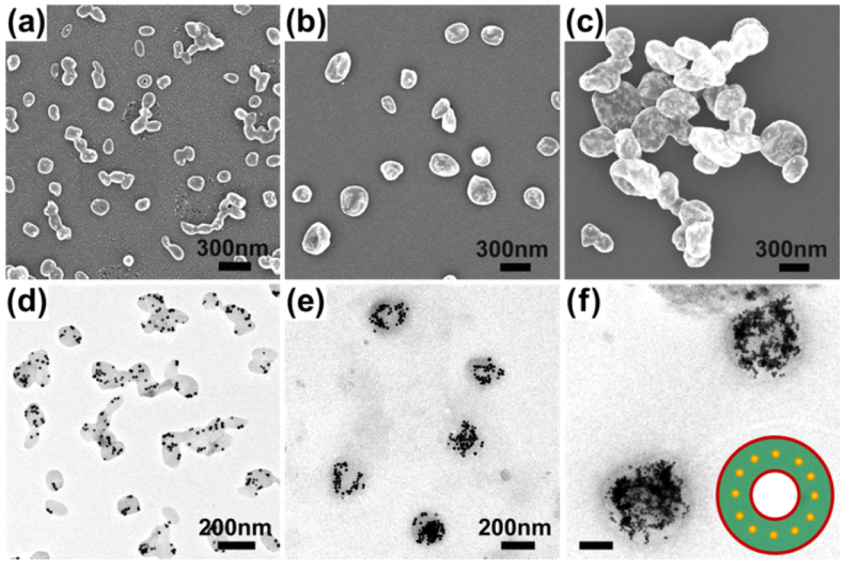

Figure 6. (a–c) SEM and (d–f) TEM images of assemblies formed by BEB/AuOAm2 mixtures with various f_{OAm2}: (a, d) 0.17, (b, e) 0.35, and (c, f) 0.50. Inset in (f) depicts the distribution of NPs in the vesicle wall. Scale bar in (f) is 200 nm.

simulations obtained similar results shown in the experiments (Figure 5a–d), except for the morphologies of the nucleated structures (rodlike in experiments vs spherical in simulations). Both the experiments and simulations demonstrate that the formation of vesicles is a process controlled by nucleation and growth.

Effect of Nanoparticle Size and Hydrophobicity on Cooperative Self-Assembly Behavior of Copolymer/Nanoparticle Mixtures. The effect of nanoparticle size on self-assembly behavior of BEB triblock copolymers is investigated by introducing larger AuNPs (AuOAm2, 18.9 nm). As revealed by SEM images, the morphology transition from ellipse to vesicle was also observed (Figure 6a–c). When f_{OAm2} = 0.17, the BEB/AuOAm2 mixture self-assembles into ellipse-like aggregates. When f_{OAm2} increases to 0.35, the ellipse-like structures disappear, and vesicles are formed. The size of the vesicles increases with f_{OAm2}. TEM images show that AuOAm2 uniformly distributes in the vesicle wall (see inset cartoon), and the density of NPs increases with f_{OAm2} (Figure 6d–f). In addition, medium-sized AuNPs (10.4 nm) were applied to cooperative self-assemble with BEB, an ellipse-to-vesicle morphology transition was also observed (details are presented in Supporting Information, Figure S5). These experiments revealed that AuNPs with a relatively wide size range (from 4.5 to 18.9 nm) can induce the ellipse-to-vesicle morphology transition. In addition, for BEB/AuOAm1 mixture, the ellipse-to-vesicle morphology transition took place at f_{OAm1} = 0.08. While for the BEB/AuOAm2 mixture, ellipse-like aggregates were formed at f_{OAm2} = 0.17, and vesicles were observed at f_{OAm2} = 0.35. This result indicated that the ellipse-to-vesicle morphology transition takes place at a higher AuNPs weight fraction if larger NPs are used.

The hydrophobicity of NPs (or the surface properties of NPs) is another important factor influencing the cooperative self-assembly behavior.[14,47] In this work, AuDT which is more hydrophobic than AuOAm1 and AuOAm2, was applied to

DOI: 10.1021/acs.langmuir.6b01484
Langmuir 2016, 32, 6917–6927

examine the effect of hydrophobicity on the cooperative self-assembly behavior of BEB/AuNPs mixtures. As shown in Figure 7, when f_{AuDT} gradually increases, a morphology

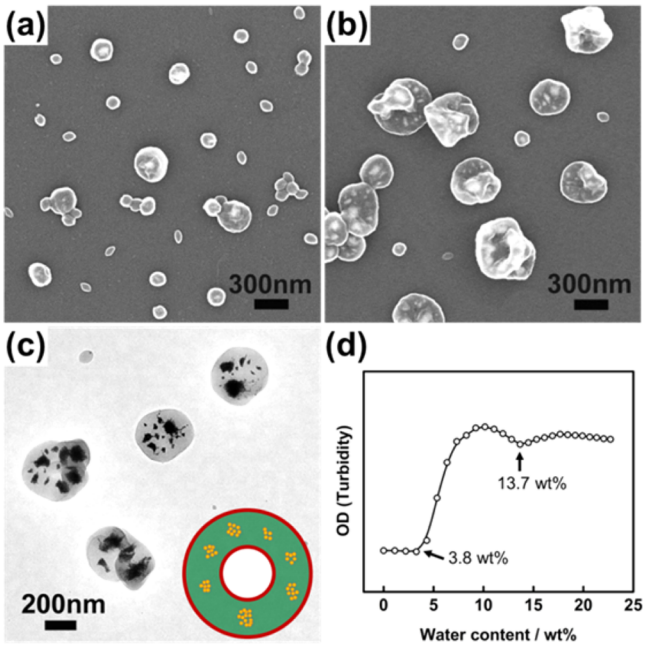

Figure 7. (a, b) SEM and (c) TEM images of the assemblies formed by BEB/AuDT mixtures with (a) f_{AuDT} = 0.10 and (b, c) f_{AuDT} = 0.30. Inset in (c) depicts the distribution of NPs in the vesicle wall. (d) Turbidity curve of BEB/AuDT mixture as a function of the amount of water added to the solutions.

transition from ellipses to a mixture of ellipses and vesicles (Figure 7a) and then to pure vesicles (Figure 7b) was observed (see details in Supporting Information, Figure S6). As can be seen from TEM image in Figure 7c, AuDT clusters rather than dispersed particles are encapsulated in the vesicle wall. Cartoon inset in Figure 7c depicts the distribution of AuNPs in the vesicle wall. The explanation of this phenomenon can be deduced from the turbidity curve of BEB/AuDT mixture (Figure 7d). As shown in the figure, aggregation of AuDT occurs at the water content of about 3.8 wt %, while assembly of BEB occurs at 13.7 wt %. This suggests that AuDT first aggregated into clusters and then cooperatively self-assembled with BEB. As a result, they were embedded in the vesicle wall in the cluster form. As compared to AuDT, AuOAm1 and AuOAm2 are less hydrophobic, their CWCs are close to that of BEB triblock copolymers (12.8 and 15.3 wt % vs 13.7 wt %). Therefore, AuOAm1 and AuOAm2 can cooperatively self-assemble with BEB in dispersed form. Both the distribution and location of NPs may critically affect the properties and potential applications of copolymer/NP assemblies. The clustered NPs in assemblies are expected to exhibit enhanced physicochemical properties, such as ultraviolet absorption and fluorescence intensity.[57] The information obtained from the present work may provide useful guidance for construction of hybrid block copolymer aggregates with specific distribution of NPs and subsequently facilitate their potential applications in biotechnology, biomedicine, catalysis, etc.[11,58]

Mechanism of the Nanoparticle-Induced Ellipse-to-Vesicle Morphology Transition of Copolymer Aggregates. Based on the experiment and simulation results, a mechanism of the ellipse-to-vesicle morphology transition induced by NPs is proposed. The BEB triblock copolymers are well dissolved in THF. When the selective solvent (water) was added, the PBLG blocks became insoluble. To reduce the exposure of the PBLG block to the selective solvents, BEB triblock copolymers self-assemble into ellipse-like aggregates, in which the PBLG rods are in a favor form of parallel arrangement. In this fashion, the PBLG can be densely packed and the interfacial energy is optimized. When NPs are introduced to cooperatively self-assemble with copolymers, the ordered packing of rigid PBLG chain in the aggregate core can be broken. Moreover, since the NPs can fill the gap between the rigid chain segments, the parallel packing of the PBLG chains is not the necessary choice to make the cores densely packed. As a consequence, vesicles are formed instead of ellipse-like aggregates. It should be noted that when a small portion of NPs is introduced, the size of the vesicles is comparable with the ellipse-like aggregates, and the interfacial energies of the vesicles can be reduced compared with those of ellipse-like aggregates with comparative sizes. When more NPs are introduced, the size of the vesicles increases, which further

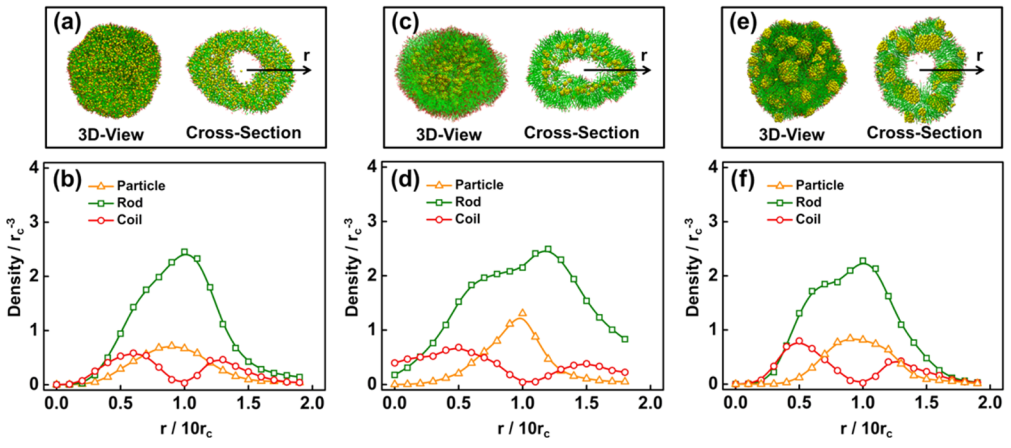

Figure 8. (a, c, e) Simulation structures and (b, d, f) density profiles for the vesicles self-assembled from the mixtures of rod−coil−rod triblock copolymers and NPs: (a, b) small NPs (AuOAm1), (c, d) larger NPs (AuOAm2), (e, f) small NPs with higher hydrophobicity (AuDT). r = 0 r_c corresponds to the vesicle center. The weight fractions of smaller and larger NPs in block copolymer/nanoparticle mixtures were set as 0.2 and 0.4, respectively.

DOI: 10.1021/acs.langmuir.6b01484
Langmuir 2016, 32, 6917−6927

lowers the interfacial energy of the system to compensate for the decrease in weight fraction of hydrophilic segments.[1]

To prove the above assumption that the NPs can fill the gaps between rigid chains, we carried out the DPD simulations on the structures formed by the mixtures of rod−coil−rod triblock copolymers and NPs (Figure 8). As can be seen from Figure 8a, the vesicle structure was observed and the NPs are localized uniformly in the vesicle wall. The parallel packing of rod blocks is disrupted owing to the size exclusion effect of NPs. We also plotted the density profiles of NPs, rod blocks, and coil blocks in the vesicle wall (Figure 8b). The unimodal profile of rod blocks and the bimodal profile of coil blocks indicate the vesicular structure, while the coincidence of the peaks corresponding to NPs and rod blocks prove the spatial distribution of NPs in the vesicle wall. Simulation results well reproduced the morphology transition observed in the experiments and provide molecular-level information such as the chain packing mode and the NP distribution.

Additionally, the effects of the size and hydrophobicity of the NPs on the self-assembly were studied by the DPD simulations. Figures 8c,d show the structure of a typical vesicle formed by rod−coil−rod triblock copolymers and larger NPs. It can be seen from Figure 8c that the NPs are located at the middle region of the vesicle wall. The density profiles of NPs, rod blocks, and coil blocks corroborate the vesicular structure of aggregates and the distribution of NPs in the vesicle wall (Figure 8d). The simulation results reveal that the larger NPs cannot fill the space between the rigid chains and instead they appear around the ends of PBLG chains. Figures 8e,f show the simulation structure of a typical vesicle formed by rod−coil−rod triblock copolymers and small NPs with higher hydrophobicity. As can be seen from Figure 8e, the NPs are aggregated within the vesicle wall due to the enhanced hydrophobicity, and the self-assembly behavior observed in experiments is reproduced. The density profiles of NPs, rod blocks, and coil blocks confirm the vesicular structure of aggregates (Figure 8f). As compared with experiments (Figures 6 and 7), it was found that the DPD simulations can well reproduce the distributions of either the large NPs or the small NPs with higher hydrophobicity in the vesicles.

Finally, we wish to emphasize the significance of this work. On the one hand, we elucidated how NPs affect the self-assembly behavior of rod−coil BCPs. The results reveal that the NPs play different role in the self-assembly of rod−coil BCP system from that of the coil−coil BCP system. In the coil−coil BCP system, the NPs can increase the effective volume taken up by hydrophobic domain. While in the rod−coil BCP system, the role of NPs is manifested in the breakage of ordered and dense packing of rod blocks. Both our previous work and the reports in the literature revealed that the rod−coil type block copolymers can self-assemble into vesicles when the rod blocks are not orderly packed.[29,59] In this work, we observed an ellipse-to-vesicle morphology transition, which is attributed to the disruption of orientation order of the rods by NPs. Meanwhile, we also examined the effect of PBLG length on the self-assembly behaviors of BEB. It was found that the copolymers with relatively longer PBLG rods self-assemble into ellipse-like aggregates. When the PBLG becomes shorter, vesicles are observed. This can be explained by the fact that the orientation order is reduced as rod blocks become shorter. Therefore, both ellipse-to-vesicle morphology transitions can be attributed to the same mechanism; i.e., the ordered packing of PBLG chains is disrupted either by NPs or decreasing of rod block length. However, in the present work, we focused on the morphology transition induced by NPs. The mechanism is well revealed by experiment and simulations. On the other hand, among the different block copolymer vesicles studied so far, polypeptide-based vesicles present several advantages, such as biocompatible, biodegradable, and mechanical stability due to the rodlike conformation of polypeptide chains forming the hydrophobic part of the vesicle.[39] In addition, inorganic NPs are able to endow the hybrid vesicle with novel functions. To date, there are few examples of hybrid vesicles self-assembled from polypeptide-based copolymer and inorganic NPs. The present work not only deepens our understanding of the self-assembly behavior of rod−coil BCPs but also provides a new way of constructing polypeptide-based hybrid vesicles in aqueous solution.

CONCLUSIONS

We employed experimental methods and DPD simulations to investigate the cooperative self-assembly behavior of PBLG-*b*-PEG-*b*-PBLG (BEB) rod−coil−rod polypeptide triblock copolymers and AuNPs. Pure BEB triblock copolymers with relatively longer PBLG rods self-assemble into ellipse-like aggregates, and DPD simulation revealed that PBLG rods tend to take parallel and dense packing fashion in the core of the ellipse-like aggregates. A morphology transition from ellipse-like aggregates to vesicles occurs when AuNPs are introduced. The effect of size and hydrophobicity of the AuNPs on self-assembly behavior was elucidated. It was found that larger AuNPs can also induce such an ellipse-to-vesicle morphology transition at a higher AuNPs weight fraction. When AuNPs are more hydrophobic, they are dispersed in the vesicle wall in a cluster form. The main reason for the ellipse-to-vesicle transition is attributed to the breakage of ordered and dense packing of PBLG rods. The results gained from the studies provide a useful guidance for constructing hybrid polypeptide vesicles with controllable size and nanoparticle distribution, which may have potential applications in bioengineering, medical therapy and high-performance catalysis.

ASSOCIATED CONTENT

Supporting Information

The Supporting Information is available free of charge on the ACS Publications website at DOI: 10.1021/acs.langmuir.6b01484.

Synthesis, characterization of triblock copolymers and gold nanoparticles, effect of PBLG length, electron microscopy images of the aggregate morphologies self-assembled from mixture system, simulation details (PDF)

AUTHOR INFORMATION

Corresponding Authors

*E-mail jlin@ecust.edu.cn (J.L.).
*E-mail caichunhua@ecust.edu.cn (C.C.).

Notes

The authors declare no competing financial interest.

ACKNOWLEDGMENTS

This work was supported by the National Natural Science Foundation of China (21234002, 21474029, 51303055, and 51573049) and the National Basic Research Program of China (2012CB933600). Support from projects of Shanghai munic-

DOI: 10.1021/acs.langmuir.6b01484
Langmuir 2016, 32, 6917−6927

ipality (15QA1401400, 15ZZ028, and 13JC1402000) and Fundamental Research Funds for the Central Universities (22A201514001) is also appreciated.

REFERENCES

(1) Mai, Y.; Eisenberg, A. Self-assembly of block copolymers. *Chem. Soc. Rev.* **2012**, *41*, 5969−5985.
(2) Hudson, Z. M.; Boott, C. E.; Robinson, M. E.; Rupar, P. A.; Winnik, M. A.; Manners, I. Tailored hierarchical micelle architectures using living crystallization-driven self-assembly in two dimensions. *Nat. Chem.* **2014**, *6*, 893−898.
(3) Cai, C.; Lin, J. Self-assembly: Served on a nanoplate. *Nat. Chem.* **2014**, *6*, 857−858.
(4) Chen, L.; Jiang, T.; Lin, J.; Cai, C. Toroid formation through self-assembly of graft copolymer and homopolymer mixtures: Experimental studies and dissipative particle dynamics simulations. *Langmuir* **2013**, *29*, 8417−8426.
(5) Chen, L.; Jiang, T.; Cai, C.; Wang, L.; Lin, J.; Cao, X. Polypeptide-based "smart" micelles for dual-drug delivery: A combination study of experiments and simulations. *Adv. Healthcare Mater.* **2014**, *3*, 1508−1517.
(6) Bakshi, M. S. Colloidal micelles of block copolymers as nanoreactors, templates for gold nanoparticles, and vehicles for biomedical applications. *Adv. Colloid Interface Sci.* **2014**, *213*, 1−20.
(7) Zhu, W.; Cai, C.; Lin, J.; Wang, L.; Chen, L.; Zhuang, Z. Polymer micelle-directed growth of $BaCO_3$ spiral nanobelts. *Chem. Commun.* **2012**, *48*, 8544−8546.
(8) Pippa, N.; Kaditi, E.; Pispas, S.; Demetzos, C. PEO-b-PCL-DPPC chimeric nanocarriers: self-assembly aspects in aqueous and biological media and drug incorporation. *Soft Matter* **2013**, *9*, 4073−4082.
(9) Di Corato, R.; Bigall, N. C.; Ragusa, A.; Dorfs, D.; Genovese, A.; Marotta, R.; Manna, L.; Pellegrino, T. Multifunctional nanobeads based on quantum dots and magnetic nanoparticles: Synthesis and cancer cell targeting and sorting. *ACS Nano* **2011**, *5*, 1109−1121.
(10) Kim, T.; Hyeon, T. Applications of inorganic nanoparticles as therapeutic agents. *Nanotechnology* **2014**, *25*, 012001.
(11) Sarkar, B.; Alexandridis, P. Block copolymer−nanoparticle composites: Structure, functional properties, and processing. *Prog. Polym. Sci.* **2015**, *40*, 33−62.
(12) Kang, Y.; Taton, T. A. Controlling shell thickness in core-shell gold nanoparticles via surface-templated adsorption of block copolymer surfactants. *Macromolecules* **2005**, *38*, 6115−6121.
(13) Hickey, R. J.; Haynes, A. S.; Kikkawa, J. M.; Park, S.-J. Controlling the self-assembly structure of magnetic nanoparticles and amphiphilic block-copolymers: From micelles to vesicles. *J. Am. Chem. Soc.* **2011**, *133*, 1517−1525.
(14) Luo, Q.; Hickey, R. J.; Park, S.-J. Controlling the location of nanoparticles in colloidal assemblies of amphiphilic polymers by tuning nanoparticle surface chemistry. *ACS Macro Lett.* **2013**, *2*, 107−111.
(15) Wang, M.; Zhang, M.; Li, J.; Kumar, S.; Walker, G. C.; Scholes, G. D.; Winnik, M. A. Self-assembly of colloidal quantum dots on the scaffold of triblock copolymer micelles. *ACS Appl. Mater. Interfaces* **2010**, *2*, 3160−3169.
(16) Yusuf, H.; Kim, W.-G.; Lee, D. H.; Guo, Y.; Moffitt, M. G. Size control of mesoscale aqueous assemblies of quantum dots and block copolymers. *Langmuir* **2007**, *23*, 868−878.
(17) Hoheisel, T. N.; Hur, K.; Wiesner, U. B. Block copolymer−nanoparticle hybrid self-assembly. *Prog. Polym. Sci.* **2015**, *40*, 3−32.
(18) Zhang, L.; Lin, J.; Lin, S. Self-assembly behavior of amphiphilic block copolymer/nanoparticle mixture in dilute solution studied by self-consistent-field theory/density functional theory. *Macromolecules* **2007**, *40*, 5582−5592.
(19) Xu, J.; Han, Y.; Cui, J.; Jiang, W. Size selective incorporation of gold nanoparticles in diblock copolymer vesicle wall. *Langmuir* **2013**, *29*, 10383−10392.
(20) Ma, Z.; Li, R. K. Y. Effect of particle surface selectivity on composite nanostructures in nanoparticle/diblock copolymer mixture dilute solution. *J. Colloid Interface Sci.* **2011**, *363*, 241−249.
(21) Ma, S.; Qi, D.; Xiao, M.; Wang, R. Controlling the localization of nanoparticles in assemblies of amphiphilic diblock copolymers. *Soft Matter* **2014**, *10*, 9090−9097.
(22) Zhang, J.; Chen, X.-F.; Wei, H.-B.; Wan, X.-H. Tunable assembly of amphiphilic rod−coil block copolymers in solution. *Chem. Soc. Rev.* **2013**, *42*, 9127−9154.
(23) Olsen, B. D.; Segalman, R. A. Self-assembly of rod−coil block copolymers. *Mater. Sci. Eng., R* **2008**, *62*, 37−66.
(24) Cai, C.; Li, Y.; Lin, J.; Wang, L.; Lin, S.; Wang, X.-S.; Jiang, T. Simulation-assisted self-assembly of multicomponent polymers into hierarchical assemblies with varied morphologies. *Angew. Chem., Int. Ed.* **2013**, *52*, 7732−7736.
(25) Agut, W.; Taton, D.; Brulet, A.; Sandre, O.; Lecommandoux, S. Depletion induced vesicle-to-micelle transition from self-assembled rod−coil diblock copolymers with spherical magnetic nanoparticles. *Soft Matter* **2011**, *7*, 9744−9750.
(26) Piñol, R.; Jia, L.; Gubellini, F.; Lévy, D.; Albouy, P.-A.; Keller, P.; Cao, A.; Li, M.-H. Self-assembly of PEG-*b*-liquid crystal polymer: The role of smectic order in the formation of nanofibers. *Macromolecules* **2007**, *40*, 5625−5627.
(27) Zhang, J.; Lin, W.; Liu, A.; Yu, Z.; Wan, X.; Liang, D.; Zhou, Q. Solvent effect on the aggregation behavior of rod−coil diblock copolymers. *Langmuir* **2008**, *24*, 3780−3786.
(28) Li, X.; Gao, Y.; Xing, X.; Liu, G. Polygonal micellar aggregates of a triblock terpolymer containing a liquid crystalline block. *Macromolecules* **2013**, *46*, 7436−7442.
(29) Zhuang, Z.; Cai, C.; Jiang, T.; Lin, J.; Yang, C. Self-assembly behavior of rod−coil−rod polypeptide block copolymers. *Polymer* **2014**, *55*, 602−610.
(30) Reuther, J. F.; Siriwardane, D. A.; Campos, R.; Novak, B. M. Solvent tunable self-assembly of amphiphilic rod−coil block copolymers with chiral, helical polycarbodiimide segments: Polymeric nanostructures with variable shapes and sizes. *Macromolecules* **2015**, *48*, 6890−6899.
(31) Cai, C.; Lin, J.; Zhu, X.; Gong, S.; Wang, X.-S.; Wang, L. Superhelices with designed helical structures and temperature-stimulated chirality transitions. *Macromolecules* **2016**, *49*, 15−22.
(32) Huang, Y.; Mai, Y.; Yang, X.; Beser, U.; Liu, J.; Zhang, F.; Yan, D.; Müllen, K.; Feng, X. Temperature-dependent multidimensional self-assembly of polyphenylene-based "rod−coil" graft polymers. *J. Am. Chem. Soc.* **2015**, *137*, 11602−11605.
(33) Cai, C.; Wang, L.; Lin, J.; Zhang, X. Morphology transformation of hybrid micelles self-assembled from rod−coil block copolymer and nanoparticles. *Langmuir* **2012**, *28*, 4515−4524.
(34) Barmatov, E. B.; Pebalk, D. A.; Barmatova, M. V. Influence of silver nanoparticles on the phase behavior of side-chain liquid crystalline polymers. *Langmuir* **2004**, *20*, 10868−10871.
(35) Lu, H.; Wang, J.; Song, Z.; Yin, L.; Zhang, Y.; Tang, H.; Tu, C.; Lin, Y.; Cheng, J. Recent advances in amino acid *N*-carboxyanhydrides and synthetic polypeptides: chemistry, self-assembly and biological applications. *Chem. Commun.* **2014**, *50*, 139−155.
(36) Ray, J. G.; Johnson, A. J.; Savin, D. A. Self-assembly and responsiveness of polypeptide-based block copolymers: How "Smart" behavior and topological complexity yield unique assembly in aqueous media. *J. Polym. Sci., Part B: Polym. Phys.* **2013**, *51*, 508−523.
(37) Zhuang, Z.; Zhu, X.; Cai, C.; Lin, J.; Wang, L. Self-assembly of a mixture system containing polypeptide graft and block copolymers: Experimental studies and self-consistent field theory simulations. *J. Phys. Chem. B* **2012**, *116*, 10125−10134.
(38) Schlaad, H. Solution properties of polypeptide-based copolymers. *Adv. Polym. Sci.* **2006**, *202*, 53−73.
(39) Zhao, L.; Li, N.; Wang, K.; Shi, C.; Zhang, L.; Luan, Y. A review of polypeptide-based polymersomes. *Biomaterials* **2014**, *35*, 1284−1301.

DOI: 10.1021/acs.langmuir.6b01484
Langmuir 2016, 32, 6917−6927

(40) Huang, J.; Bonduelle, C.; Thévenot, J.; Lecommandoux, S.; Heise, A. Biologically active polymersomes from amphiphilic glycopeptides. *J. Am. Chem. Soc.* **2012**, *134*, 119−122.
(41) Iatrou, H.; Frielinghaus, H.; Hanski, S.; Ferderigos, N.; Ruokolainen, J.; Ikkala, O.; Richter, D.; Mays, J.; Hadjichristidis, N. Architecturally induced multiresponsive vesicles from well-defined polypeptides. Formation of gene vehicles. *Biomacromolecules* **2007**, *8*, 2173−2181.
(42) Blout, E. R.; Karlson, R. H. Polypeptides. III. The synthesis of high molecular weight poly-γ-benzyl-L-glutamates1. *J. Am. Chem. Soc.* **1956**, *78*, 941−946.
(43) Peng, S.; Lee, Y.; Wang, C.; Yin, H.; Dai, S.; Sun, S. A facile synthesis of monodisperse Au nanoparticles and their catalysis of CO oxidation. *Nano Res.* **2008**, *1*, 229−234.
(44) Hiramatsu, H.; Osterloh, F. E. A simple large-scale synthesis of nearly monodisperse gold and silver nanoparticles with adjustable sizes and with exchangeable surfactants. *Chem. Mater.* **2004**, *16*, 2509−2511.
(45) Brust, M.; Walker, M.; Bethell, D.; Schiffrin, D. J.; Whyman, R. Synthesis of thiol-derivatised gold nanoparticles in a two-phase liquid−liquid system. *J. Chem. Soc., Chem. Commun.* **1994**, *0*, 801−802.
(46) Komolkin, A. V.; Laaksonen, A.; Maliniak, A. Molecular dynamics simulation of a nematic liquid crystal. *J. Chem. Phys.* **1994**, *101*, 4103−4116.
(47) Kim, Y.-J.; Cho, C.-H.; Paek, K.; Jo, M.; Park, M.-k.; Lee, N.-E.; Kim, Y.-j.; Kim, B. J.; Lee, E. Precise control of quantum dot location within the P3HT-*b*-P2VP/QD nanowires formed by crystallization-driven 1D growth of hybrid dimeric seeds. *J. Am. Chem. Soc.* **2014**, *136*, 2767−2774.
(48) Lynd, N. A.; Meuler, A. J.; Hillmyer, M. A. Polydispersity and block copolymer self-assembly. *Prog. Polym. Sci.* **2008**, *33*, 875−893.
(49) Zhou, Z.; Li, Z.; Ren, Y.; Hillmyer, M. A.; Lodge, T. P. Micellar shape change and internal segregation induced by chemical modification of a tryptych block copolymer surfactant. *J. Am. Chem. Soc.* **2003**, *125*, 10182−10183.
(50) Cai, C.; Lin, J.; Chen, T.; Tian, X. Aggregation behavior of graft copolymer with rigid backbone. *Langmuir* **2010**, *26*, 2791−2797.
(51) Hamasaka, G.; Muto, T.; Uozumi, Y. Molecular-architecture-based administration of catalysis in water: Self-assembly of an amphiphilic palladium pincer complex. *Angew. Chem., Int. Ed.* **2011**, *50*, 4876−4878.
(52) Sun, J.; Chen, X.; Deng, C.; Yu, H.; Xie, Z.; Jing, X. Direct formation of giant vesicles from synthetic polypeptides. *Langmuir* **2007**, *23*, 8308−8315.
(53) Dai, S.; Ravi, P.; Tam, K. C.; Mao, B. W.; Gan, L. H. Novel pH-responsive amphiphilic Diblock copolymers with reversible micellization properties. *Langmuir* **2003**, *19*, 5175−5177.
(54) Wan, W.-M.; Hong, C.-Y.; Pan, C.-Y. One-pot synthesis of nanomaterials via RAFT polymerization induced self-assembly and morphology transition. *Chem. Commun.* **2009**, 5883−5885.
(55) Hashimoto, T.; Sakamoto, N. Nucleation and anisotropic growth of lamellar microdomains in block copolymers. *Macromolecules* **1995**, *28*, 4779−4781.
(56) Dong, X.-H.; Ni, B.; Huang, M.; Hsu, C.-H.; Bai, R.; Zhang, W.-B.; Shi, A.-C.; Cheng, S. Z. D. Molecular-curvature-induced spontaneous formation of curved and concentric lamellae through nucleation. *Angew. Chem., Int. Ed.* **2016**, *55*, 2459−2463.
(57) Chen, H.; Yeh, J.; Wang, L.; Khurshid, H.; Peng, N.; Wang, A.; Mao, H. Preparation and control of the formation of single core and clustered nanoparticles for biomedical applications using a versatile amphiphilic diblock copolymer. *Nano Res.* **2010**, *3*, 852−862.
(58) Mei, S.; Cao, J.; Lu, Y. Controllable assembly of two types of metal nanoparticles onto block copolymer nanospheres with ordered spatial distribution. *J. Mater. Chem. A* **2015**, *3*, 3382−3389.
(59) Lin, Y.-L.; Chang, H.-Y.; Sheng, Y.-J.; Tsao, H.-K. Self-assembled polymersomes formed by symmetric, asymmetric and side-chain-tethered coil-rod-coil triblock copolymers. *Soft Matter* **2014**, *10*, 1840−1852.

DOI: 10.1021/acs.langmuir.6b01484
Langmuir 2016, 32, 6917−6927